DALTON
FULL PAPER

Design of molecular materials combining magnetic, electrical and optical properties †

Eugenio Coronado,* Miguel Clemente-León, José R. Galán-Mascarós,‡ Carlos Giménez-Saiz, Carlos J. Gómez-García and Eugenia Martínez-Ferrero

Departamento de Química Inorgánica, Universidad de Valencia, Dr. Moliner 50, E-46100 Burjasot, Spain. E-mail: eugenio.coronado@uv.es

Received 27th April 2000, Accepted 5th July 2000
First published as an Advance Article on the web 25th September 2000

The possibilities offered by hybrid functional materials formed by two molecular networks in the context of crystal engineering are illustrated with two different examples: (i) hybrid magnets constructed from combination of an extended ferromagnetic or ferrimagnetic inorganic network, with a molecular paramagnetic metal complex acting as template. (ii) Hybrid organic–inorganic compounds combining an organic π-electron donor network that furnishes the pathway for electronic conductivity, with inorganic metal complexes that act as structural and/or magnetic components. These examples illustrate how this hybrid approach allows the design of molecular materials combining non-conventional magnetic, electrical and optical properties.

Introduction

"Magnetic lattice engineering" may be seen as an active subarea of "crystal engineering". The concept was introduced by de Jongh in 1982 during a summer school on "*Magneto–Structural Correlations in Exchange-Coupled Systems*".[1] This new philosophy in magnetism consisted of starting to look for and, if necessary, to synthesize the materials one needed for a given purpose, instead of studying magnetic properties of materials 'as available' in nature. This approach had a great impact among the chemical community which continues today. In the initial steps, chemists were interested in the molecular design and synthesis of simple magnetic systems of low dimensionality (dimers, chains) with the aim to use them as model systems to test the physical theories and models existing in magnetism, as well as to establish useful magneto–structural correlations.[2] With this background chemists became more interested in increasing the structural and magnetic complexities of systems with the aim to control, as much as possible, the passage from molecular properties to collective phenomena, from molecular assemblies to magnetic materials and from molecular engineering to crystal engineering.[3] During the last fifteen years or so the "star" materials in this area have been the molecule-based magnets and a variety of novel lattices have been discovered and/or modified both in organic and inorganic chemistries taking advantage of the versatility of molecular chemistry.[4] Very recently several attempts have been made to add complexity to the magnetic systems by constructing materials in which magnetic properties are combined with other physical properties (electrical, optical, photophysical, *etc.*).[5] A suitable molecular approach to reach this goal is to design two-network materials such as host–guest solids or cation–anion salts, where each network furnishes distinct physical properties.[6] Here, we use this concept to construct hybrid magnets formed by two magnetic networks, and hybrid compounds combining an organic π-electron donor network that furnishes the pathway for electronic conductivity, with inorganic metal complexes that act as structural and/or magnetic components.

Results and discussion

1. Controlling the crystal dimensionality of a polymeric coordination network through a molecular network. The design of hybrid molecular magnets

It is well known that extended magnetic networks of dimensionalities two (2-D) and three (3-D) can be chemically constructed from oxalato-bridged bimetallic complexes.[7] These coordination polymers behave as ferro-,[8] ferri-[9] or canted antiferromagnets[10,11] with critical temperatures (T_c) ranging from 5 up to 44 K. They are formed when a bulky cation is added to an aqueous solution containing the molecular precursors $[M^{III}(ox)_3]^{3-}$ and $M^{2+}(aq)$ [or $M^{+}(aq)$]. The insoluble salt so obtained combines an extended anion network (the bimetallic complex) with a molecular cation which plays the role of template as it controls the connectivity between the two metal complexes and thus the type of crystal structure. At the same time this cation can be electronically active and thus it can add complexity and interest to the resulting material. Such a possibility allows us to design novel functional materials with interesting magnetic properties or combinations of properties.[6b] Here, we focus on the crystal chemistry and magnetic properties of those materials that contain a paramagnetic complex as a molecular cation.

The 2-D series. This series is formed with bulky organic monocations of the type $[XR_4]^+$. The compounds have the formula $[XR_4][M^{II}M^{III}(ox)_3]$ (M^{II} = Mn, Fe, Co, Ni, Cu, Zn; M^{III} = Cr, Fe, Ru; X = N, P; R = *n*-alkyl, phenyl...). The first examples of these phases were reported by Okawa and coworkers in 1990.[12] The crystal structures of these compounds contain honeycomb layers of octahedral M^{II} and M^{III} tris(oxalate) sites connected through the oxalate ligand.[13] These anion layers are interleaved by layers of organic cations. The formation of the honeycomb layer requires adjacent M^{II} and M^{III} sites to have opposite configuration (Δ and Λ) (Fig. 1). Recently we have shown that organometallic monocations of the type $[FeCp^*_2]^+$ (decamethylferrocenium) can also stabilize

† Based on the presentation given at Dalton Discussion No. 3, 9–11th September 2000, University of Bologna, Italy.
Dedicated to Professor Oliver Kahn. In memoriam.
‡ Present address: Department of Chemistry, Texas A&M University, College Station, USA.

DOI: 10.1039/b003396k

This journal is © The Royal Society of Chemistry 2000

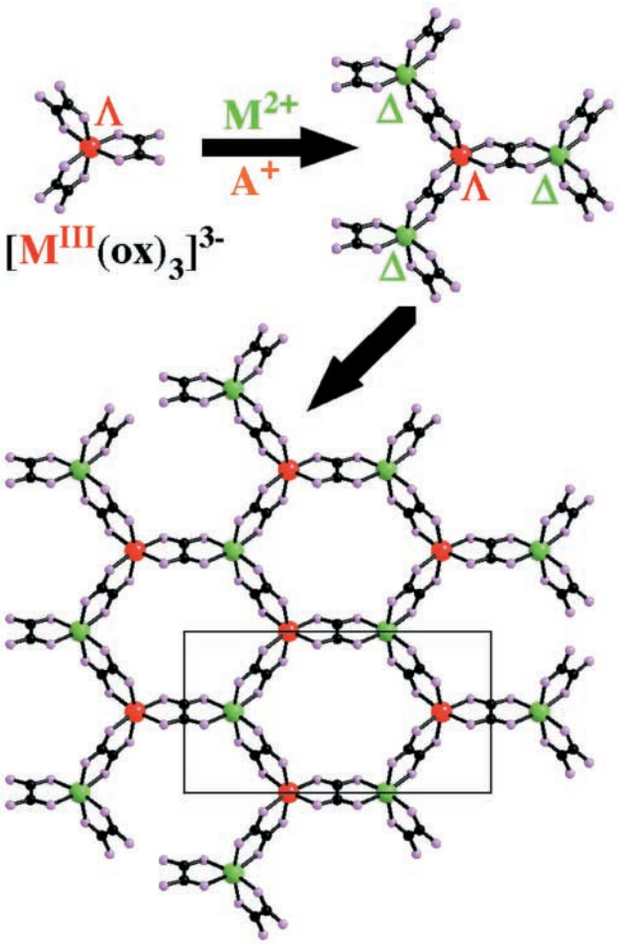

Fig. 1 Schematic construction of the 2-D layers by combination of alternating Λ and Δ isomers of tris(oxalato)metalate complexes in the presence of the bulky monocation A^+.

the honeycomb layers, despite the very different geometry of these cations compared with $[XR_4]^+$.[14] Such an approach has led to a new family of organometallic–inorganic magnetic compounds of formula $[Z^{III}Cp^*_2][M^{II}M^{III}(ox)_3]$ (Z^{III} = Fe, Co or Mn; M^{II} = Mn, Fe, Co, Ni, Cu, Zn; M^{III} = Cr, Fe). It is of interest in the context of crystal engineering to compare the structural features in all these materials. All of them maintain the honeycomb layer network but the stacking of the layers is strongly dependent on the nature of the cation. Thus, with the $[ZCp^*_2]^+$ derivatives all the inorganic layers are of the same type and are eclipsed to each other creating hexagonal channels within which the organometallic cations are located (Fig. 2). By contrast, X-ray structures of the $[XR_4]^+$ derivatives have shown stackings with two or more inorganic layers in the unit cell,[15] while layer disorder due to stacking faulting has often been found in polycrystalline powders.[16] These different stackings are probably connected with the different symmetry of the inserted cation as well as with the way in which it is placed with respect to the two surrounding layers. Thus, in the $[XR_4]^+$ derivatives we often observe that one of the four arms of the organic cation penetrates into one of the two neighboring layers but not into the other (Fig. 3, top). With these organic cations the only example in which the layers are eclipsed has been found in a $N(n\text{-}C_5H_{11})_4^+$ salt in which the four arms of the cation do not penetrate into the layers (Fig. 3, center). However, owing to the lack of an inversion center in the NR_4 unit, the two adjacent layers cannot be equivalent and then the packing has a two-layer [a–b] repeat structure. In the $[ZCp^*_2]^+$ derivatives the organometallic cation does not penetrate into the layers. Additionally, the existence of an inversion center in this cation allows it to adopt a symmetrical position with respect to the

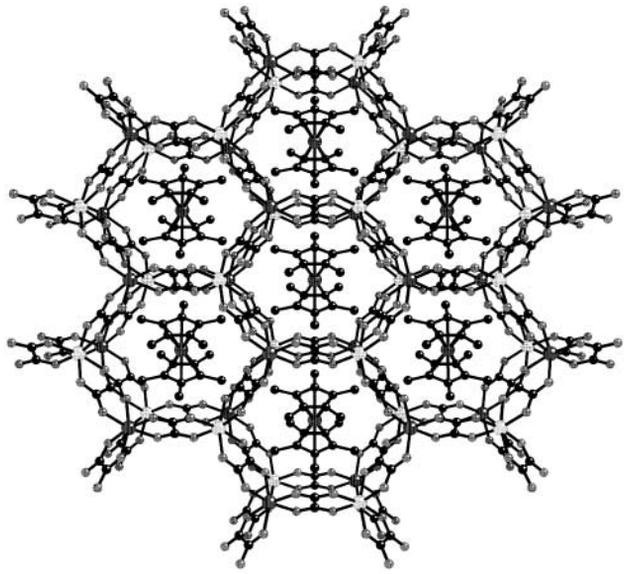

Fig. 2 Perspective view of the eclipsed 2-D layers in the family of hybrid layered magnets $[ZCp_2^*][M^{II}M^{III}(ox)_3]$ (Z^{III} = Co, Fe and Mn; M^{III} = Fe and Cr; M^{II} = Mn, Fe, Co, Ni and Cu).

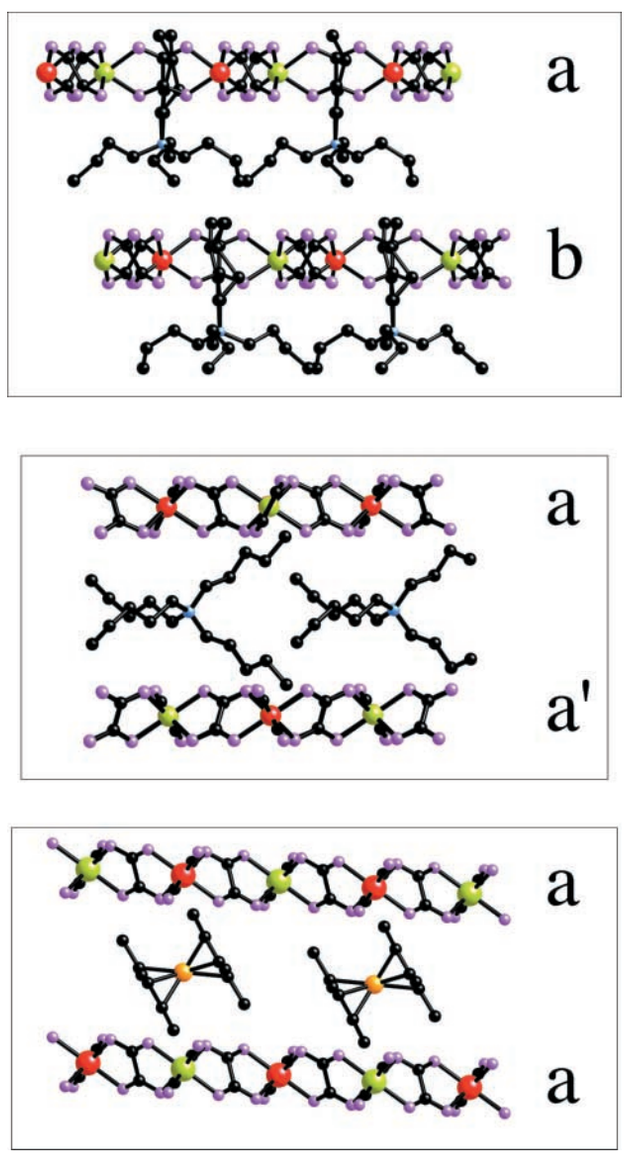

Fig. 3 (Top) Side view of the alternating (a–b) layers in the compound $[NBu_4][MnFe(ox)_3]$; (center) side view of the eclipsed (a–a′) layers in the compound $[N(n\text{-}C_5H_{11})_4][MnFe(ox)_3]$; (bottom) side view of the eclipsed (a–a) layers in the family of compounds $[ZCp_2^*][M^{II}M^{III}(ox)_3]$.

Table 1 Magnetic parameters for the series $[CoCp^*_2][M^{II}M^{III}(ox)_3]$, $[FeCp^*_2][M^{II}M^{III}(ox)_3]$, $[MnCp^*_2][M^{II}M^{III}(ox)_3]$ and $[NBu_4][M^{II}M^{III}(ox)_3]$: critical temperature ($T_c$) and coercive field ($H_{coer}$) at 2 and 5 K (in parentheses)

	$CoCp^*_2$		$FeCp^*_2$		$MnCp^*_2$		NBu_4	
$M^{II}M^{III}$	T_c/K	H_{coer}/G	T_c/K	H_{coer}/G	T_c/K	H_{coer}/G	T_c/K	H_{coer}
MnCr	5.1	40 (−)	5.3	20 (10)	5.3	150 (30)	6	(20)
FeCr	12.7	1940 (760)	13.0	1100 (330)	13.0	2230 (780)	12	(320)
CoCr	8.2	250 (50)	9.0	130 (50)	9.3	170 (25)	10	(80)
CuCr	6.7	200 (20)	7.0	180 (40)	7.0	390 (95)	7	(30)
MnFe	25.4	150 (150)	28.4	120 (40)	27.8	750 (390)	28	—
FeFe	44.0	100 (100)	43.3	370 (1240)	45.0	26 (9)	45	—

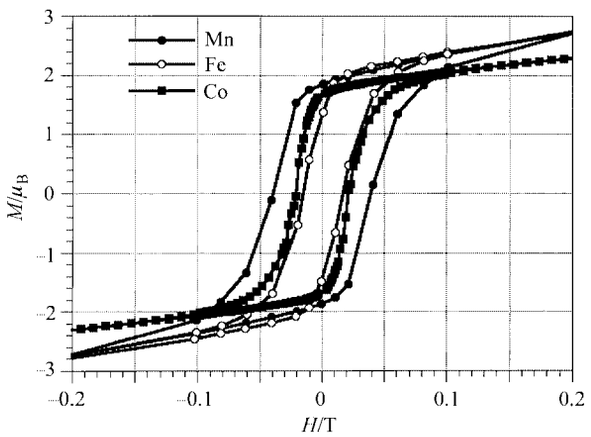

Fig. 4 Hysteresis loops for the $[ZCp_2^*][CuCr(ox)_3]$ family of ferromagnets (Z^{II} = Co, Fe and Mn).

two nearest layers; therefore, an eclipsed stacking of equivalent layers is possible in which the two pentamethylcyclopentadienyl molecules of the $[ZCp^*_2]^+$ cation point towards the center of the hexagons (Fig. 3, bottom).

The different stackings of the magnetic layers may have consequences in the bulk magnetic properties of the materials. However, at first sight, the relevant magnetic parameters of the $[FeCp^*_2]^+$ molecular magnets, *i.e.* the critical temperatures and coercive fields, are found to be roughly the same that those observed in the $[XR_4]^+$ derivatives.[14b] This result emphasizes that in these layered magnets the long-range magnetic ordering is essentially 2-D as it is controlled by the interactions within the bimetallic layers. In order to examine whether the nature of the organometallic cation influences the bulk magnetism of the layered material we have inserted three different cations, $[CoCp^*_2]^+$, $[FeCp^*_2]^+$ and $[MnCp^*_2]^+$ in between the bimetallic layers resulting in diamagnetic (Co) or paramagnetic (Fe, Mn) cations. We observe that the nature of the cations has little influence on the ordering temperatures (Table 1) while some influence is exerted on the coercive fields. For example, in the $[Cu^{II}Cr^{III}]$ series H_c varies from 180 G when the paramagnetic cation $[FeCp^*_2]^+$ ($S = 1/2$) is inserted, to 400 G when $[MnCp^*_2]^+$ ($S = 1$) is inserted (Fig. 4). When the diamagnetic cation $[CoCp^*_2]^+$ is inserted, an intermediate H_c value of 200 G is observed.

The 3-D series. A second type of bimetallic network is formed when chiral cations such as $[Z^{II}(bpy)_3]^{2+}$ (Z^{II} = Fe, Co, Ni, Ru, Zn) are used in which a chiral three-dimensional structure is formed with general formula $[Z^{II}(bpy)_3][M^IM^{III}(ox)_3]$ or $[Z^{II}(bpy)_3][M^{II}M^{II}(ox)_3]$ (M^{II} = Mn, Fe, Co, Cu; M^{III} = Cr, Fe; M^I = alkali metal, NH_4^+). These phases were first reported by Decurtins *et al.* in 1993.[17] In contrast to the previous layered phases, in the 3-D phases the two metal sites, M^{III} and M^I, have the same configuration (Δ or Λ) and so the network is chiral (Fig. 5). The polymeric structure contains cavities in which the $[Z^{II}(bpy)_3]^{2+}$ are located. These cavities have some flexibility and

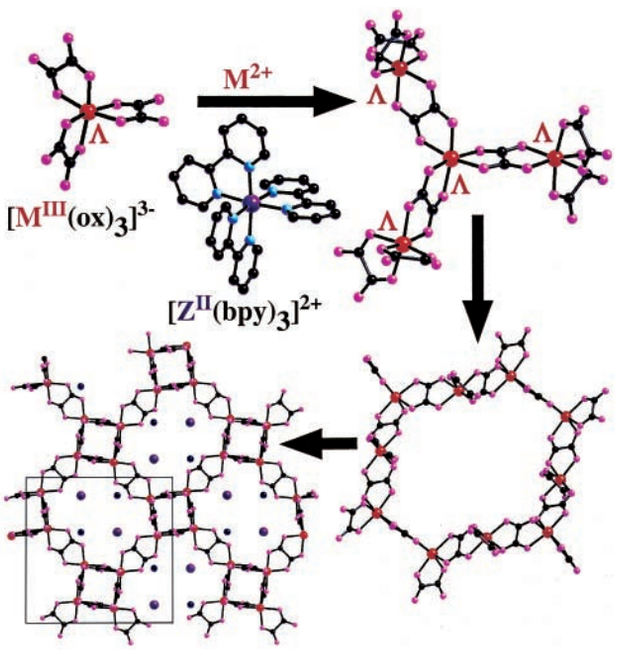

Fig. 5 Schematic construction of the 3-D network $[M^{II}M^{III}(ox)_3]^-$ by combination of Λ (or Δ) isomers of tris(oxalato) metalate complexes in the presence of a chiral metal complex Λ-$[Z(bpy)_3]^{2+}$ ($Z = Co^{II}$, Fe^{II}, Mn^{II}, Ni^{II} and Ru^{II}) acting as template.

can also accommodate small monoanions X^- (= ClO_4^-, BF_4^- or PF_6^-). This feature allows extension of the range of compounds that can be obtained with formula $[Z^{II}(bpy)_3][X][M^{II}M^{III}(ox)_3]$. From the magnetic point of view, only the homometallic $[M^{II}M^{II}]$ and the bimetallic $[M^{II}M^{III}]$ series are magnetically interesting as they can give rise to magnetic ordered phases. The $[M^IM^{III}]$ series behave as simple paramagnets since the magnetic M^{III} centers are surrounded by diamagnetic alkali ions, M^I. Unfortunately, the preparation of pure $[M^{II}M^{III}]$ materials has been synthetically challenging. The most serious obstacle is that M^I ions can also enter in the 3-D structure; therefore, all the compounds prepared in presence of these ions lead to impure 3-D lattices containing significant amounts of diamagnetic M^I ions in place of M^{II}. To solve this problem we have used the silver salt as the source of chromium tris(oxalate) complex. Reaction of this salt with the corresponding M^{II} chloride leads to the immediate precipitation of AgCl and to a solution free from monocations. Addition of $[Z^{II}(bpy)_3]^{2+}$ complexes to this solution then leads to the formation of the desired hybrid magnet. Table 2 summarizes the magnetic parameters of the series $Z^{II}[Mn^{II}Cr^{III}]$ (Z^{II} = Fe, Co, Ni, Ru). These compounds are ferromagnets with critical temperatures ranging from $T_c < 2$ K for the Ru derivative to 3.9 K for the Fe derivative. The ferromagnetic nature of the interactions can be deduced from dc magnetic measurements which show positive Weiss constants (Table 2). T_c values can be determined through ac magnetic susceptibilities, measurements of which show a maximum in the in-phase signal (χ') near T_c and an out-of-

Table 2 Magnetic parameters for the series $[Z(bpy)_3][ClO_4][MnCr(ox)_3]$; values of M and H_{coer} are at 2 K

Z(II)	M(II)	T_c/K	θ/K	C/emu K mol^{-1}	M/μ_B (5 T)	H_{coer}/G
Ru	Mn	<2.0	5.0	5.9	6.7	5
Fe	Mn	3.9	4.2	6.2	6.0	0
Ni	Mn	2.3	2.6	6.6	7.7	13
Co	Mn	2.2	1.1	7.4	7.5	13

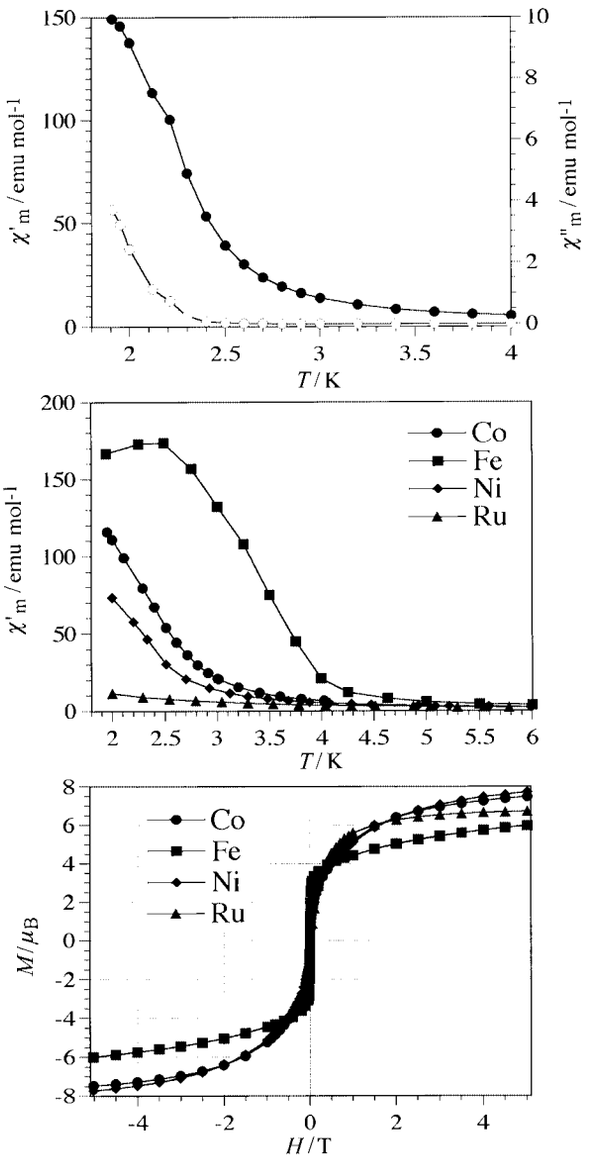

Fig. 6 (Top) Temperature dependence of the in-phase (filled symbols) and out-of-phase (open symbols) ac susceptibilities for the compound $[Co(bpy)_3](ClO_4)[MnCr(ox)_3]$; (center) in-phase susceptibility signals in the series $[Z(bpy)_3](ClO_4)[MnCr(ox)_3]$ (Z^{II} = Co, Fe, Ni and Ru); (bottom) isothermal magnetization curves *vs.* H in this series.

phase signal (χ'') that starts to appear at temperatures just below T_c (Fig. 6, top and center). Finally, S-shaped curves are observed in the magnetization *vs.* magnetic field plot at 2 K (Fig. 6, bottom) with magnetization values at 5 K which are compatible with a parallel alignment of Mn^{II} and Cr^{III} spins (5/2 and 3/2). However, the magnetic field required to approach saturation is rather large and no clear saturation of the magnetization was observed in any case. These features have already been noted in the analogous 2-D phases and are indicative of the presence of a spin canting in the ordered ferromagnetic structure. Furthermore, the coercive fields remain small in all cases (Table 2) indicating that these hybrid compounds are

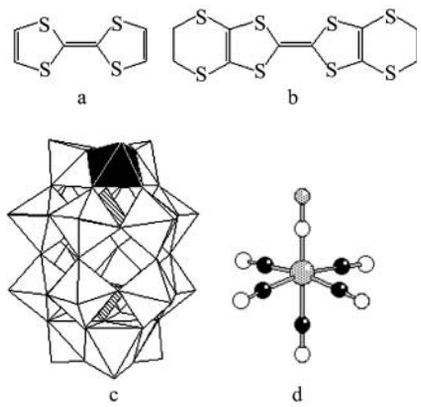

Fig. 7 Molecular ingredients used for the construction of the organic–inorganic hybrids formed by π-electron donor molecules and inorganic molecular complexes. Organic donors: TTF (a) and BEDT–TTF (b); inorganic complexes: $[ReOP_2W_{17}O_{61}]^{6-}$ polyoxometalate anion (c); nitroprusside anion (d).

very soft canted ferromagnets. It is of surprise, however, that small changes in the molecular network significantly influence the magnetic properties (T_c values) of the extended magnetic network. For example, in the $[Ru(bpy)_3]^{2+}$ derivative, T_c is below 2 K, while when smaller 3d-cations are inserted, T_c increases up to 3.9 K (in the Fe derivative). This result is in sharp contrast to the behaviour of the 2-D phases and is probably due to the larger structural flexibility of the 3-D lattice, compared to the 2-D one. The 3-D network can accommodate cations and anions of different sizes in the cavities. In addition, this structural feature probably affects intermetallic bond angles and distances in the network, and therefore the exchange interactions and ordering temperatures. In turn, in the 2-D network the insertion of different types of cations determines the interlayer separation, but does not necessarily alter the geometry within the layers or the exchange interactions. Additionally, the magnetic nature of the cation complex does not seem to affect the magnetic ordering temperature. Thus, no change in T_c is observed when the paramagnetic Ni ($S = 1$) is replaced by the anisotropic Co complex ($S = 3/2$), despite the change in size and anisotropy of the spin. To summarize we can state that both the 2-D and 3-D series provide nice examples of molecular-based magnets, and that the bulk magnetic properties of the 3-D lattice can be tuned by varying the size of the inserted molecular complex. These series of magnets are also of interest owing to their chirality. In this context, they should provide the opportunity to investigate the interplay between optical activity and ferromagnetism (Faraday and Kerr effects). This aspect will be explored in the near future.

2. Controlling the crystal packing of π-electron donor molecules through inorganic molecular complexes. The design of hybrid materials with coexistence of conductivity and magnetism

Radical cation salts formulated as $[Donor]_mX_n$ are typically formed by segregated stacks of partially oxidized π-electron donors of the tetrathiafulvalene (TTF)-type [Fig. 7(a) and (b)] interleaved by charge-compensating inorganic anions X^- such as Cl^-, Br^-, I_3^-, PF_6^-, AsF_6^-, BF_4^-, ClO_4^- or NO_3^-. These low dimensional solids have provided many examples of molecular conductors and superconductors.[18] A current development in this area is to explore the novel lattice architectures and physical properties resulting from the association of these organic donors with large molecular anions that possess "active" electrons. We present here an example that illustrates the ability of these types of anions to induce novel packings in the organic network and to incorporate an additional electronic component to the material.

The studied example incorporates as the inorganic component the polyoxoanion $[ReOP_2W_{17}O_{61}]^{6-}$ which contains a

paramagnetic Re^{VI} ion ($S = 1/2$). This anion has two central belts of six WO_6 octahedra capped by two groups of three octahedra sharing edges with two internal tetrahedral sites which are occupied by P^V atoms [Fig. 7(c)]. The rhenium ion is located in one of the six octahedra of the caps. The anion belongs to an extensive class of metal–oxide clusters termed polyoxometalates. These inorganic compounds have been found to be extremely versatile building blocks for the construction of organic–inorganic hybrids as the crystal structures of these solids are the result of the tendency of the planar organic molecules to stack and that of the inorganic clusters to adopt closed-packed lattices.[19] The combination of $[ReOP_2W_{17}O_{61}]^{6-}$ with bis(ethylenedithio)tetrathiafulvalene [BEDT-TTF, Fig. 7(b)] leads to the radical salt $(BEDT\text{-}TTF)_{11}[ReOP_2W_{17}O_{61}]\cdot 3H_2O$. The compound is obtained by electro-oxidation of the organic donor in presence of the polyanion in a solution mixture of CH_2Cl_2–DMF–DMSO–MeOH (7 : 3 : 2 : 1) after 3 weeks at a constant current of 1.2 A. This hybrid salt is isostructural with the diamagnetic $[P_2W_{18}O_{62}]^{6-}$ derivative for which the crystal structure has been already reported.[20] The present salt crystallizes in the monoclinic space group $P2_1/m$ ($a = 14.597$, $b = 42.271$, $c = 18.418$ Å) and the structure consists of alternating layers of closed-packed polyoxoanions and BEDT-TTF radicals [Fig. 8(a)]. The organic layer is formed by parallel chains of BEDT-TTF molecules which adopt a β-packing mode [Fig. 8(c)], with six crystallographically independent BEDT–TTF molecules also present [A, B, C, D, E and F in Fig. 8(b)]. Another important structural feature relates to the short interatomic contacts at the organic–inorganic interface. Hydrogen bond formation is observed between the ethylene groups of the BEDT–TTF donors and some oxygen atoms of the surface of the cluster. The oxygen atoms involved in these C–H···O hydrogen bonds mainly belong to the octahedra of the caps, in which the Re atom is located. Each of the six crystallographically independent BEDT–TTF molecules forms at least one C–H···O hydrogen bond, with C···O distances ranging from 3.1(1) to 3.4(1) Å.

A second type of interaction occurs between some S atoms of the BEDT–TTF molecules and oxygen atoms of the belts of the polyoxoanion. Again, each crystallographically independent BEDT–TTF molecule forms S···O contacts with the polyoxoanion, with S···O distances ranging from 2.80(7) to 3.23(6) Å. These structural features illustrate well the ability of polyoxometalates to induce novel crystal packings in the organic network creating, at the same time, unusual electronic distributions in the organic sublattice.

In terms of transport properties, this novel salt shows a metallic-like behavior in the region 250–300 K with an increase in the conductivity from *ca.* 11.3 S cm^{-1} at room temperature to 11.8 S cm^{-1} at 250 K. Below 250 K the salt becomes a semiconductor with the conductivity reaching a value of 1.9 S cm^{-1} at 80 K (Fig. 9). The behavior is typical of a semiconductor with a very low activation energy and closely resembles that of the $[P_2W_{18}O_{62}]^{6-}$ derivative.[20] Such a high conductivity is very rare in polyoxometalate-based radical salts with most exhibiting a strong electron localization caused by the presence of crystallographically different organic donors in the crystal as a result of the high charges and sizes of the inorganic clusters. In the present salt, however, the 2-D β-packing adopted by the BEDT–TTF radicals seems to overcome these limitations. In terms of the magnetic properties, this salt shows paramagnetic behavior in agreement with the presence of spin $S = 1/2$ rhenium(VI). The product of the molar magnetic susceptibility and the temperature (χT) has an approximately constant value of 0.45 emu K mol^{-1} down to 30 K, and decreases below this temperature to reach a value of 0.34 emu K mol^{-1} at 2 K (Fig. 10, top). EPR spectra confirm the presence of this paramagnetic ion. Thus, at high temperatures we observe an isotropic and narrow signal centered at $g = 2.006$ with a linewidth of 20 G (Fig. 10, center) which arises from the organic network.

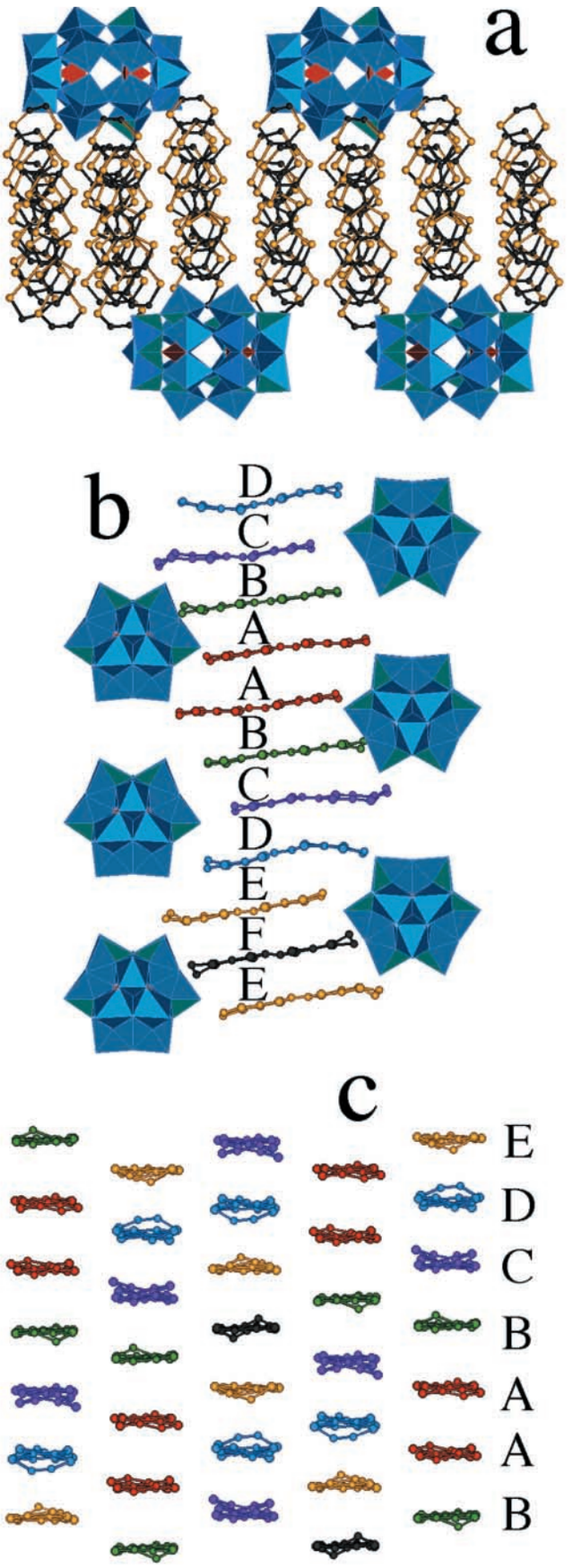

Fig. 8 $(BEDT\text{–}TTF)_{11}[ReOP_2W_{17}O_{61}]\cdot 3H_2O$: (a) structure of the radical salt showing the presence of organic layers BEDT–TTF alternating with inorganic layers of the paramagnetic cluster anion $[ReOP_2W_{17}O_{61}]^{6-}$; (b) view of the stacking of the organic chains with labels on the different BEDT–TTF cations; (c) structure of the organic layer showing the β-packing of the BEDT–TTF molecules.

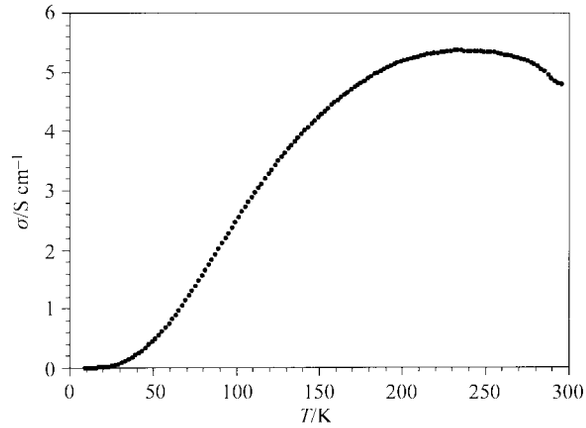

Fig. 9 $(BEDT–TTF)_{11}[ReOP_2W_{17}O_{61}]\cdot 3H_2O$: temperature dependence of the dc electrical conductivity in the plane of the organic layers.

Below 100 K a complex spectrum with many signals distributed over the range 1000–6000 G is superimposed on the initial spectrum and increases in intensity upon cooling and dominates in the low temperature region. Indeed at 4.5 K, we observe the typical spectrum of Re^{VI} in a rhombic environment imposed by the polyoxometalate framework (Fig. 10, bottom), with signals that can be simulated from a spin-Hamiltonian that considers Zeeman, hyperfine and nuclear quadrupole interactions.[21] No influence of the organic sublattice on this spectrum is detected. Thus, we can conclude that the two electronic networks are independent. In the polyoxometalate area, this organic/inorganic salt constitutes the best known example of coexistence of localized magnetic moments with highly delocalized electrons.

Other combinations are also being explored in this area, for example, the combination of TTF-type donors with the nitroprusside complex $[Fe(CN)_5(NO)]^{2-}$ [Fig. 7(d)]. This diamagnetic anion is photochromic and exhibits photoinduced transitions to extremely long-lived metastable states[22] accompanied by a change in the geometry of the complex. Such a feature may affect the conductive properties of the radical salt. On the other hand, any interaction of the NO ligand with the organic environment should considerably affect this light-induced process. Metallic and semiconducting radical salts of this anion with BEDT–TTF and TTF, respectively, have recently been reported.[23,24]

Conclusions

The above results have shown that the hybrid approach is a most successful procedure to prepare new types of molecule-based materials combining two or more functional properties, which is a current challenge in materials science. However, this approach is still in its infancy. For example, we know how to obtain molecular hybrids with coexistence of localized and itinerant electrons, but the preparation of molecular materials combining two cooperative properties such as ferromagnetism and electrical conductivity, or even superconductivity, remains a challenge. The advance in the preparation of molecular hybrids with useful physical properties will depend not only upon serendipity or from a trial and error procedure, but also from a crystal engineering effort that involves two main aspects namely: (i) the development of convenient synthetic strategies leading to a better control of the supramolecular architecture of the material, and (ii) a detailed study, both from experimental and theoretical points of view, of the intermolecular interactions present in the solid, paying particular attention to the interphase between the two molecular networks, and to the correlation between these interactions and the electronic properties of the material.

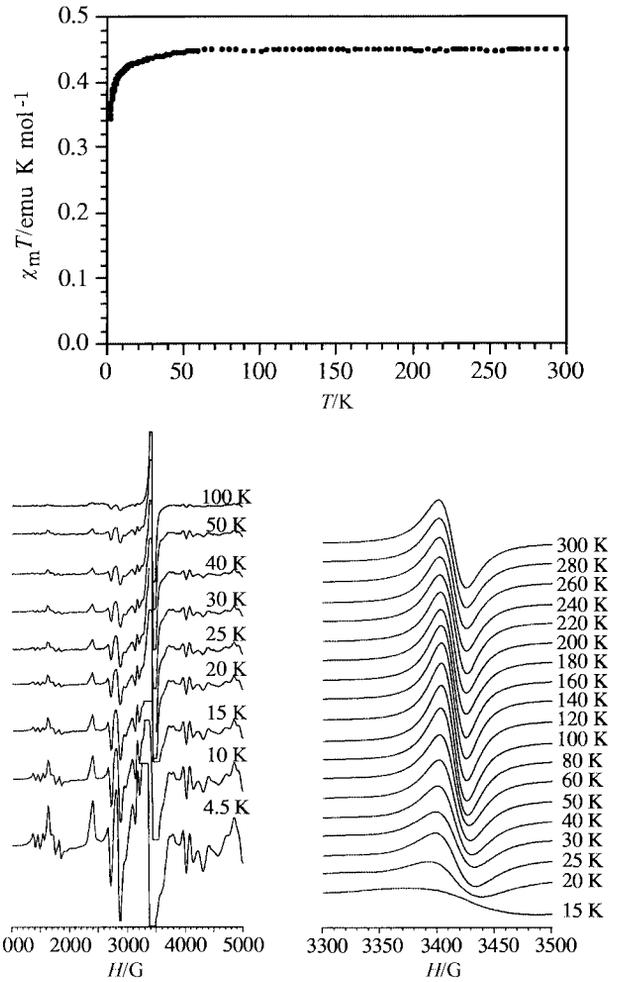

Fig. 10 Magnetic properties of $(BEDT–TTF)_{11}[ReOP_2W_{17}O_{61}]\cdot 3H_2O$: (top) temperature dependence of χT. (bottom) EPR spectra as a function of the temperature.

Experimental

Magnetic measurements

Magnetic susceptibility measurements (ac and dc) were carried out on polycrystalline samples between 2 and 300 K in a magnetometer equipped with a SQUID sensor (Quantum Design MPMS-XL-5). Low temperature isothermal magnetization measurements were performed on the same apparatus in the presence of a magnetic field between −5 and 5 T.

EPR spectroscopy

Measurements on polycrystalline samples were performed between 4.2 and 300 K with a X-band Bruker ELEXSYS E500 spectrometer equipped with a liquid helium cryostat.

Electrical conductivity

dc Electrical conductivities were measured on single crystals with a Keithley 224 current source capable of generating a continuous current between 5 μA and 0.1 A, and with a Keithley 2182 nanovoltmeter, with a maximum sensitivity of 1 nV. Equipment from the SQUID magnetometer was used for cryogenic measurements.

Acknowledgements

We thank Professor V. Lauhkin for performing the electrical conductivity measurements reported in this work. Financial support from Spain (Grant MAT98/0880) and the European Union (Network ERBFMRXCT 980181 on Molecular

Magnetism: From Materials Toward Devices) is gratefully acknowledged. C. G.-S. and E. M.-F. thank the MEC for a research contract (Contrato de Reincorporación) and for a fellowship grant, respectively.

References

1 L. J. de Jongh, in *Magneto-Structural Correlations in Exchange-Coupled Systems*, eds. R. D. Willett, D. Gatteschi and O. Kahn, Reidel, Dordrecht, NATO-ASI Series, 1983, vol. C-140, pp. 1–36.
2 O. Kahn, *Molecular Magnetism*, VCH, New York, 1993
3 *Molecular Magnetism: From Molecular Assemblies to the Devices*, eds. E. Coronado, P. Delhaes, D. Gatteschi and J. S. Miller, Kluwer Academic Publishers, Dordrecht, NATO ASI Series, 1996, vol. E-321; *Magnetism: A Supramolecular Function*, ed. O. Kahn, Kluwer Academic Publishers, Dordrecht, NATO ASI Series, 1996, vol. C-484.
4 P. Day, *Science*, 1993, **261**, 431.
5 M. Clemente-León, E. Coronado, P. Delhaes, J. R. Galán Mascarós, C. J. Gómez-García and C. Mingotaud, in *Supramolecular Engineering of Synthetic Metallic Materials. Conductors and Magnets*, eds. J. Veciana, C. Rovira and D. B. Amabilino, Kluwer Academic Publishers, Dordrecht, NATO ASI Series, 1998, vol. C518, pp. 291–312.
6 (*a*) M. Clemente-León, E. Coronado, J. R. Galán-Mascarós, C. J. Gómez-García, C. Rovira and V. N. Lauhkin, *Synth. Met.*, 1999, **103**, 2339; (*b*) E. Coronado, J. R. Galán-Mascarós and C. J. Gómez-García, *Mol. Cryst. Liq. Cryst.*, 1999, **334**, 679.
7 S. Decurtins, R. Pellaux, A. Hauser and M. E. Von Arx, in *Magnetism: A Supramolecular Function*, ed. O. Kahn, Kluwer Academic Publishers, Dordrecht, NATO ASI Series, 1996, vol. C-484, p. 487.
8 H. Tamaki, Z. J. Zhong, N. Matsumoto, S. Kida, M. Koikawa, N. Achiwa, Y. Hashimoto and H. Okawa, *J. Am. Chem. Soc.*, 1992, **114**, 6974.
9 H. Tamaki, M. Mitsumi, K. Nakamura, N. Matsumoto, S. Kida, H. Okawa and S. Iijima, *Chem. Lett.*, 1992, 1975; J. Larionova, B. Bombelli, J. Sanchiz and O. Kahn, *Inorg. Chem.*, 1998, **37**, 679.
10 C. Mathonière, J. Nuttall, S. G. Carling and P. Day, *Inorg. Chem.*, 1996, **35**, 1201.
11 M. Hernández-Molina, F. Lloret, C. Ruiz-Pérez and M. Julve, *Inorg. Chem.*, 1998, **37**, 4131.
12 Z.-J. Zhong, N. Matsumoto, H. Okawa and S. Kida, *Chem. Lett.*, 1990, 87.
13 L. O. Atovmyan, G. V. Shilov, R. N. Lyubovskaya, E. I. Zhilyaeva, N. S. Ovanesyan, S. I. Pirumova and I. G. Gusakovskaya, *JETP Lett.*, 1993, **58**, 766; S. Decurtins, H. W. Schmalle, H. R. Oswald, A. Linden, J. Ensling, P. Gütlich and A. Hauser, *Inorg. Chim. Acta*, 1994, **216**, 65.
14 (*a*) M. Clemente-León, E. Coronado, J. R. Galán-Mascarós and C. J. Gómez-García, *Chem. Commun.*, 1997, 1727; (*b*) E. Coronado, J. R. Galán-Mascarós, C. J. Gómez-García, J. Ensling and P. Gütlich, *Chem. Eur. J.*, 2000, **6**, 552.
15 R. Pellaux, H. W. Schmalle, R. Huber, P. Fisher, T. Hauss, B. Ouladdiaf and S. Decurtins, *Inorg. Chem.*, 1997, **36**, 2301; S. G. Carling, C. Mathonière, P. Day, K. M. Abdul Malik, S. J. Coles and M. B. Hursthouse, *J. Chem. Soc.*, *Dalton Trans.*, 1996, 1839.
16 C. J. Nutall and P. Day, *J. Solid State Chem.*, 1999, **147**, 3.
17 S. Decurtins, H. W. Schmalle, P. Schneuwly and H. R. Oswald, *Inorg. Chem.*, 1993, **32**, 1888; S. Decurtins, H. W. Schmalle, P. Schneuwly, J. Ensling and P. Gütlich, *J. Am. Chem. Soc.*, 1994, **116**, 9521.
18 J. M. Williams, J. R. Ferraro, R. J. Thorn, K. D. Carlson, U. Geiser, H. H. Wang, A. M. Kini and M. H. Whangbo, *Organic Superconductors: Synthesis*, *Structure*, *Properties and Theory*, Prentice Hall, Englewood Cliffs, NJ, 1992.
19 E. Coronado and C. J. Gomez-Garcia, *Chem. Rev.*, 1998, **98**, 273.
20 E. Coronado, J. R. Galán-Mascarós, C. Giménez-Saiz, C. J. Gómez-García and V. N. Laukhin, *Adv. Mater.*, 1996, **8**, 801.
21 A. Venturelli, M. J. Nilges, A. Smirnov, R. L. Belford and L. C. Francesconi, *J. Chem. Soc.*, *Dalton Trans.*, 1999, 301.
22 U. Hauser, V. Oestreich and H. D. Rohrweck, *Z. Phys.*, 1977, **17**, A280; Th. Woike, W. Krasser, P. S. Bechthold and S. Haussühl, *Phys. Rev. Lett.*, 1984, **53**, 1767.
23 L. A. Kushch, L. Buratov, V. Tkacheva, E. B. Yagubskii, L. Zorina, S. Khasanov and R. Shibaeva, *Synth. Met.*, 1999, **102**, 1646 (Proceedings of the ICSM'98); M. Gener, E. Canadell, S. S. Kashanov, L. V. Zorina, R. P. Shibaeva, L. A. Kushch and E. B. Yagubskii, *Solid State Commun.*, 1999, **111**, 329.
24 M. Clemente-León, E. Coronado, J. R. Galán-Mascarós, C. Giménez-Saiz, C. J. Gómez-García and J. M. Fabre, *Synth. Met.*, 1999, **103**, 2279 (Proceedings of the ICSM'98).